HHS Public Access

Author manuscript

Nat Struct Mol Biol. Author manuscript; available in PMC 2011 October 01.

Published in final edited form as:

Nat Struct Mol Biol. 2011 April ; 18(4): 486–492. doi:10.1038/nsmb.2031.

Dominant Prion Mutants Induce Curing Through Pathways That Promote Chaperone-Mediated Disaggregation

Susanne DiSalvo, **Aaron Derdowski**, **John A. Pezza**, and **Tricia R. Serio***

Brown University, Department of Molecular Biology, Cell Biology and Biochemistry, 185 Meeting St., Box G-L2, Providence, RI 02912, USA

Abstract

Protein misfolding underlies many neurodegenerative diseases, including the Transmissible Spongiform Encephalopathies (prion diseases). While cells typically recognize and process misfolded proteins, prion proteins evade protective measures by forming stable, self-replicating aggregates. However, co-expression of dominant-negative prion mutants can overcome aggregate accumulation and disease progression through currently unknown pathways. Here, we determine the mechanisms by which two mutants of the *Saccharomyces cerevisiae* Sup35 protein cure the [*PSI*$^+$] prion. We show that both mutants incorporate into wildtype aggregates and alter their physical properties in different ways, diminishing either their assembly rate or their thermodynamic stability. While wildtype aggregates are recalcitrant to cellular intervention, mixed aggregates are disassembled by the molecular chaperone Hsp104. Thus, rather than simply blocking misfolding, dominant-negative prion mutants target multiple events in aggregate biogenesis to enhance their susceptibility to endogenous quality control pathways.

Cellular phenotypes are established, in large part, by the collective activities of their unique proteomes, and alterations to the physical state of individual proteins, such as changes in conformation, have the capacity to induce dramatic phenotypic switches. The prototypical conformation-based phenotypes are those associated with prion proteins, which have been implicated in a number of distinct biological phenomena including transmissible neurodegenerative diseases in mammals, heritable traits in fungi, and synaptic efficiency in an invertebrate.[1] These changes in cellular function, however, can only emerge if the misfolded prion proteins persist and are amplified to levels that perturb normal cellular homeostasis. Accumulation of misfolded prion proteins is facilitated by their assembly into ordered aggregates, which not only protect these aberrant species from refolding or degradation but also template the conversion of other forms of the protein to a like state.[1] This conformational self-replication, along with the continuous fragmentation of aggregates into smaller complexes, mediates an exponential increase in misfolded prion protein over the course of disease.[2]

*To whom correspondence should be addressed, Tricia_Serio@Brown.edu.

Author Contributions

SD and TRS designed the experiments, analyzed the data and wrote the manuscript, and SD, AD, and JAP performed the experiments.

The efficient and autocatalytic pathway of prion protein misfolding provides a molecular explanation for the progressive nature of prion diseases, but it also complicates their effective treatment, which would require the complete resolution of existing aggregates. This challenge, however, may not be insurmountable. Naturally occurring polymorphisms in the mammalian prion protein PrP alter the pathological and clinical characteristics of prion diseases.[1] In most of these cases, heterozygosity at the PrP locus mitigates the severity of disease.[3–9] In addition, differences in prion protein sequence confer strain-dependent resistance to infection and to the transmission of disease between species,[10–21] and co-expression of some allelic combinations reduces or eliminates the accumulation of misfolded PrP *in vivo*.[22–26] Intriguingly, the severity of these dominant-negative effects is dependent upon the relative stoichiometry of mutant and wildtype protein, and different mutants can be distinguished by the ratios at which they become effective inhibitors.[23,27,28]

Given the central role of misfolded prion protein in the appearance, maintenance and spread of prion-associated phenotypes, dominant-negative prion mutants are thought to inhibit the self-replicated misfolding of wildtype prion protein. In this scenario, the observed ratio effects can be explained as differences in affinity, with the mutants inhibiting the conversion of wildtype prion protein to the misfolded form through direct binding.[22,27,29] However, distinct effective inhibitory ratios may also indicate that individual mutants interfere with prion propagation through unique pathways. For example, mutants that target the conversion step are predicted to act efficiently at substoichiometric levels given the limited number of templating surfaces on an aggregate, while mutants that alter fragmentation or transmission of aggregates may act only at higher concentrations where they incorporate into these complexes at levels sufficient to alter their properties.[30]

Here, we use the Sup35/[*PSI*$^+$] system of *Saccharomyces cerevisiae* to uncover the mechanisms by which dominant-negative prion mutants inhibit prion propagation *in vivo*. [*PSI*$^+$] is a self-replicating misfolded (prion) form of the translation release factor Sup35.[1] Under normal conditions, Sup35 is synthesized and rapidly converted to the prion form in a [*PSI*$^+$] strain by interaction with and incorporation into existing aggregates.[31] The molecular chaperones Hsp104, Hsp70 (Ssa1) and Hsp40 (Sis1) must then fragment these aggregates, by extracting and unfolding constituent Sup35 monomers, to generate additional templates for conversion and to ensure their efficient transfer to daughter cells.[32–38] This misfolding partially compromises Sup35 function, leading to a defect in translation termination that can be easily scored in yeast strains encoding genes with nonsense mutations. For example, [*PSI*$^+$] strains carrying the *ade1–14* allele form white colonies on rich and adenine-deficient media due to readthrough of a premature stop codon in the *ADE1* open reading frame, but strains with defective prion propagation, or those that have lost the prion state ([*psi*$^-$]), form red colonies on rich medium and fail to grow in the absence of adenine due to the accumulation of active, non-prion state Sup35.[35]

For these studies, we focused on two dominant-negative prion mutants, the [*PSI*$^+$]-no-more (PNM) variants, Q24R and G58D (also known as PNM2).[39–41] These substitutions map to two different elements in the bipartite Sup35 prion-determining domain, the glutamine and asparagine-rich region (QNR, amino acids 1–40) and the oligopeptide-repeat region (OPR, amino acids 41–97), respectively, which are both necessary for the stable inheritance of the

[*PSI*$^+$] prion.[1] Although both mutants dominantly induce prion curing, we show that they do so by targeting distinct events in the Sup35 misfolding pathway. In both cases, these changes impact aggregate dynamics *in vivo*, ultimately promoting chaperone-mediated disassembly of existing aggregates.

Results

Effective inhibitory ratios distinguish PNM mutants

The dominant-negative effect of G58D on [*PSI*$^+$] propagation has been reported in some yeast strains but not others.[40,42] These differences may reflect distinct interactions of the mutant with each genetic background, but the previous studies also differed in the expression level of the mutant relative to wildtype Sup35. To explore the possibility that PNM mutants inhibit prion propagation in a dose-dependent manner, we generated diploid [*PSI*$^+$] yeast strains expressing wildtype Sup35 at different ratios relative to the PNM mutants G58D and Q24R (2:1, 1:1, 1:2; see Supplementary Fig. 1). Expression of G58D at any ratio in a [*PSI*$^+$] strain eliminated growth on adenine-deficient medium, indicating reversal of the prion phenotype (Fig. 1a). By colony color, the severity of this effect increased with G58D dosage, with a wildtype-to-mutant ratio of 1:2 displaying a colony phenotype that was indistinguishable from the [*psi*$^-$] state (Fig. 1a). The dominant-negative effect of Q24R expression on the [*PSI*$^+$] colony phenotype also increased with its dosage, but the prion colony color phenotype was suppressed even at the substoichiometric ratio (2:1 wildtype-to-mutant; Fig. 1a).

To determine if reversal of the [*PSI*$^+$] phenotype upon PNM expression reflected prion loss (curing), we analyzed [*PSI*$^+$] inheritance in the wildtype meiotic progeny of these strains. For G58D, [*PSI*$^+$] inheritance was largely stable at the substoichiometric (0% curing) and equal ratios (3% curing), where the colony color phenotype was only mildly reversed (Fig. 1a, b). However, [*PSI*$^+$] did not appear in wildtype meiotic progeny when G58D was expressed in excess of wildtype Sup35 in the parental diploid (1:2 wildtype-to-mutant; 100% curing; Fig. 1b), consistent with the complete reversal of the prion phenotype (Fig. 1a). For Q24R, which had a more severe effect on the prion phenotype (Fig. 1a), 30% of wildtype meiotic progeny lost [*PSI*$^+$] even at the substoichiometric ratio (2:1 wildtype-to-mutant), and this instability increased with its dosage (Fig. 1b). Thus, [*PSI*$^+$] curing in diploids expressing PNM mutants parallels the severity of the phenotypic reversal in these strains, and PNM mutants, like their mammalian counterparts, can be distinguished by their effective inhibitory ratios.

PNM mutants target multiple events in prion propagation

The distinct effective inhibitory ratios for G58D and Q24R may reflect differences in affinity for a single event in the Sup35 misfolding pathway or, alternatively, interference with different steps in this process. To distinguish between these possibilities, we first determined whether G58D or Q24R expression altered conversion of Sup35 to the prion form by analyzing their ability to incorporate into wildtype aggregates *in vivo*. In haploid strains, wildtype and PNM Sup35 did not interact in non-prion [*psi*$^-$] cells, as expected, but both the G58D and Q24R proteins were specifically co-immunoprecipitated with HA-tagged

wildtype Sup35 in [*PSI*$^+$] cells (Fig. 2a). Previous studies *in vivo* have demonstrated G58D aggregation in [*PSI*$^+$] strains,[42] but studies *in vitro* disagree on whether this variant can efficiently convert to the prion form.[43,44] To assess the efficiency of G58D and Q24R conversion to the prion form *in vivo*, we monitored the appearance of stop codon readthrough in zygotes formed by mating a [*psi*$^-$] strain expressing a fluorescent reporter of translation termination efficiency (GST-UGA-DsRed) to a [*PSI*$^+$] strain. Production of fluorescent protein reflects the quantitative and rapid incorporation of soluble Sup35 into aggregates and the concomitant reduction in its activity.[31] In a cross between G58D [*psi*$^-$] and wildtype [*PSI*$^+$] strains, the frequency of fluorescent zygotes was similar to a wildtype cross (~80%, Fig. 2b); however, the intensity of this fluorescence was ~20% lower in the mutant cross (Fig. 2c), consistent with a previous study suggesting a mild conversion defect for G58D.[43] In contrast, we observed fluorescence in only ~40% of zygotes resulting from a cross between Q24R [*psi*$^-$] and wildtype [*PSI*$^+$] strains, indicating a strong conversion defect for Q24R *in vivo* (Fig. 2b).

Next, we determined whether incorporation of PMN Sup35s into wildtype aggregates altered the efficiency with which they are fragmented *in vivo*. Because this process is altered by the thermodynamic stability of aggregates,[45] we assessed the sensitivity of these complexes, isolated from haploid strains expressing a 1:1 wildtype-to-mutant ratio (see Supplementary Fig. 2a, b), to disruption with 2% (w/v) SDS at different temperatures.[31] Expression of G58D did not alter the fraction of total soluble Sup35 recovered at 50°C, where aggregates remain intact (Fig. 2d).[31] However at both 60°C and 70°C, the amount of total soluble Sup35 increased by a factor of ~2.5 in comparison with a wildtype strain (Fig. 2d), indicating destabilization of the aggregates by G58D incorporation. For a strain expressing Q24R, a similar increase in total soluble Sup35 was detected at all temperatures in comparison with a wildtype strain (Fig. 2d), suggesting that Q24R expression did not alter the thermodynamic stability of aggregates but rather led to the accumulation of soluble Sup35 *in vivo*. Thus, the different effective inhibitory ratios of the PNM mutants correspond to alterations of distinct events in the Sup35 misfolding pathway *in vivo*, with G58D primarily altering the fragmentation step and Q24R affecting the conversion step.

PNM mutants alter propagon accumulation but not transmission

Modulation of the rates of conversion and fragmentation correlate with differences in the size, number, and transmissibility of aggregates *in vivo* and thereby the stability of prion-associated phenotypes.[46] To determine the mechanism(s) by which PNM mutants dominantly induce [*PSI*$^+$] loss, we assessed the effects of their expression on each of these parameters.

To determine the aggregate size distribution, we analyzed lysates of haploid strains expressing both wildtype and G58D or Q24R Sup35s by semi-denaturing detergent agarose gel electrophoresis (SDD-AGE).[47] For strains expressing either mutant, the size distribution of SDS-resistant aggregates was shifted to smaller complexes relative to wildtype strains (Fig. 3a). This effect was more severe for Q24R, consistent with the enhanced frequency of prion loss (Fig. 1b) and increased accumulation of soluble Sup35 in strains expressing this mutant in comparison with G58D (Fig. 2d). Similar effects were also observed in strains

expressing a Q24K but not a Q24N or a Q24A allele (see Supplementary Fig. 2b–d), suggesting that positive charge at this position mediated the dominant inhibition.

To determine if these changes in aggregate size correlated with the number of heritable prion units (propagons), we genetically determined these values for haploid strains expressing an extra copy of wildtype, Q24R or G58D *SUP35* (see Supplementary Fig. 2a, b) using an *in vivo* dilution assay.[48] For the wildtype strain, the median number of propagons was ~100 (Fig. 3b), and expression of Q24R and G58D had opposing effects on this baseline. For strains expressing Q24R, the median number of propagons decreased by a factor of ~7 (Fig. 3b), consistent with both the decreased proportion of aggregated Sup35 (Fig. 2d) and the increased frequency of [*PSI*$^+$] loss (Fig. 1b). In contrast, the median number of propagons increased by a factor of ~2 in the G58D strain relative to the wildtype strain (Fig. 3b). This observation is consistent with the idea that G58D incorporation increases the efficiency of aggregate fragmentation, but it also indicates that the increased frequency of [*PSI*$^+$] loss in this strain (Fig. 1b) cannot be explained by a failure to generate sufficient propagons.

To determine if G58D induces prion curing by altering the efficiency of aggregate transmission, we used a fluorescence loss in photobleaching (FLIP) assay in strains expressing Sup35-GFP-labeled aggregates.[46] For this analysis, we continually bleach either mother or daughter cells prior to cytokinesis, and monitor loss of fluorescence in the other cell as a proxy for protein transmission (see Supplementary Fig. 3). Using this assay, aggregates containing wildtype Sup35-GFP are transmitted with similar efficiencies in either direction in the presence or absence of G58D (Fig. 3c), indicating that the dominant-negative effect of this mutant also does not result from a defect in aggregate transmission.

PNM mutants promote Hsp104-mediated disassembly of aggregates

The increase in propagons and the efficient transfer of aggregates to daughter cells are difficult to reconcile with an increased frequency of [*PSI*$^+$] loss for strains expressing G58D. However, we considered the possibility that the changes in aggregate accumulation and stability induced by PNM expression (Fig. 2d) altered their interactions with other cellular components. We uncovered the molecular defects in prion propagation in haploid strains expressing both wildtype and PNM Sup35s (Figs. 2, 3), a mild over-expression of the prion protein relative to other cellular components. To determine if this imbalance impacted PNM effects, we assayed the number of propagons in diploid strains expressing either two copies of wildtype *SUP35* or one copy each of wildtype and PNM *SUP35* (see Supplementary Fig. 4a) to maintain proper expression ratios. Rather than inducing an increase in propagons as in haploids (Fig. 3b), G58D expression in diploids resulted in a reduction in propagons by a factor of ~7.5 (Fig. 4a). This enhanced inhibition of prion propagation in diploids was also apparent in a strain expressing Q24R, where the number of propagons decreased more dramatically in the diploid than in the haploid strain relative to wildtype (decrease by a factor of ~30 *vs*. ~7; Fig. 3b, 4a). Together, the strong effects of dosage on propagon accumulation suggested that other cellular factors could be mediating the biological outcomes of PNM mutant expression.

The best-characterized *trans*-regulator of [*PSI*$^+$] propagation is the molecular chaperone Hsp104. To determine if imbalance between Sup35 and Hsp104 could explain the dosage effects on PNM efficacy, we constructed heterozygous disruptions of *HSP104* in diploid strains expressing two copies of wildtype *SUP35* or one copy each of wildtype and PNM *SUP35* (see Supplementary Fig. 4a, b) to approximate our experiments in haploids. Disruption of a single copy of *HSP104* decreased the number of propagons in a wildtype strain by factor of ~1.5, consistent with its catalytic role in fragmentation (Fig. 4a).[32,33] In contrast, heterozygous disruption of *HSP104* in strains expressing either G58D or Q24R increased the number of propagons by factor of ~3–4 (Fig. 4a) and partially reversed the phenotypic effects of PNM expression (Fig. 1a), suggesting that an excess of Hsp104 activity mediated PNM inhibition of prion propagation *in vivo*. Because PNM expression did not alter Hsp104 protein levels (see Supplementary Fig. 4b,c), we hypothesized that this increase in apparent Hsp104 activity arose because it was simply functioning as a better enzyme. Specifically, the Q24R conversion defect limits the production of aggregates (Fig. 2d) and thereby skews the substrate-to-enzyme ratio, while the G58D-mediated decrease in aggregate stability (Fig. 2d) enhances fragmentation.

To experimentally determine the relationship between Hsp104 activity and PNM dominant inhibition, we compared aggregate size, as a proxy for Hsp104-mediated fragmentation efficiency,[45,47] with suppression of the [*PSI*$^+$] phenotype under various conditions. In a strain expressing a 2:1 wildtype-to-G58D ratio, heterozygous disruption of *HSP104* (see Supplementary Fig. 4c) decreased the mobility of aggregates by SDD-AGE (Fig. 4b and see Supplementary Fig. 5a), suggesting that Hsp104 activity was limiting, and this limitation suppressed the reversal of the [*PSI*$^+$] phenotype (Fig. 1a). In contrast, heterozygous disruption of *HSP104* in strains expressing a 2:1 wildtype-to-Q24R ratio or a 1:1 wildtype-to-G58D ratio led to the accumulation of both fast and slowly migrating aggregates (Fig. 4b and see Supplementary Fig. 5b), suggesting that Hsp104 activity was only partially limiting in these strains. Consistent with that idea, the heterozygous disruption of *HSP104* only partially suppressed PNM effects on the [*PSI*$^+$] phenotype in these strains (Fig. 1a) and suppressed [*PSI*$^+$] loss in the G58D but not the Q24R-expressing strain (Fig. 1b). In a strain expressing a 1:1 wildtype-to-Q24R ratio, disruption of one copy of *HSP104* failed to alter the migration of Q24R-containing aggregates (Fig. 4b and see Supplementary Fig. 4c), suggesting that Hsp104 activity remained in excess under these conditions, and, correspondingly, prion propagation remained inhibited (Fig. 1a, b). Together, these correlations strongly suggest that Hsp104-mediated fragmentation is a crucial event in the dominant inhibition of prion propagation by PNM mutants *in vivo*.

If this hypothesis is correct, prion propagation in PNM-expressing strains should be hypersensitive to excess Hsp104. To test this idea, we first determined the ratio of Sup35 and Hsp104 expression levels in [*PSI*$^+$] strains derived from two genetic backgrounds, 74-D694 and BSC783/4c, which differ in their sensitivities to G58D expression.[40,42] In the more sensitive BSC783/4c strain, Hsp104 expression is elevated by a factor of ~2.5 relative to Sup35 in comparison with 74-D694 (Fig. 4c), and the expression levels of the Hsp104 co-chaperones Ssa1 and Sis1 are also elevated in BSC783/4c (see Supplementary Fig. 6a, b). Correspondingly, aggregates in BSC783/4c were shifted to faster migrating complexes by

SDD-AGE (see Supplementary Fig. 6c), consistent with the idea that increased sensitivity to PNM inhibition correlates with elevated fragmentation activity. To rule out the possibility that this hypersensitivity resulted from other genetic differences between the two strains, we over-expressed Hsp104 to various levels (see Supplementary Fig. 4d) in 74-D694 wildtype haploid strains that co-expressed either wildtype or PNM Sup35 (see Supplementary Fig. 2a, b) and determined the frequency of [*PSI*$^+$] loss. In a strain expressing wildtype Sup35, [*PSI*$^+$] loss was only observed when Hsp104 was overexpressed by factor of ~20 ($2\mu_{PGPD}$, Fig. 4d and see Supplementary Fig. 4d). In contrast, [*PSI*$^+$] loss was observed in both G58D and Q24R expressing strains with only a single extra copy of Hsp104 ($cen_{P\mathit{104}}$), and these levels were elevated further upon overexpression of Hsp104 by a factor of ~5 and ~20 ($2\mu_{P\mathit{104}}$ and $2\mu_{PGPD}$, Fig. 4d and see Supplementary Fig. 4d). Thus, increasing Hsp104 activity can elevate the sensitivity of a [*PSI*$^+$] strain to curing by PNM mutants.

Based on this link between the strength of PNM dominant inhibition and Hsp104 activity, we hypothesized that PNM expression induces [*PSI*$^+$] curing by promoting the disassembly of aggregates *in vivo*. To monitor the fate of aggregated Sup35, we inhibited new protein synthesis by cycloheximide treatment and then determined the physical state of the existing protein at a later time point. In lysates prepared from a diploid strain expressing two wildtype copies of *SUP35*, the proportion of SDS-resistant Sup35 remained the same, indicating that previously aggregated protein remained in this fraction (Fig. 4e). In contrast, ~50% of the previously aggregated protein, isolated from a strain expressing both wildtype and either G58D or Q24R Sup35s, was resolubilized (Fig. 4e), indicating that incorporation of PNM mutants promotes aggregate disassembly *in vivo.*

Because G58D and Q24R mediate their dominant-negative effects on [*PSI*$^+$] propagation by targeting distinct events, we reasoned that combining these mutations into a single polypeptide would create an even more potent inhibitor. Indeed, the colony color of a [*PSI*$^+$] haploid strain expressing a Q24R/G58D double mutant was red in contrast with the pink color of colonies formed from strains expressing either single mutant (see Supplementary Fig. 2a, b). Moreover, [*PSI*$^+$] was lost during mitotic division in a strain expressing Q24R/G58D at a greatly enhanced frequency relative to strains expressing either the Q24R (by a factor of ~6) or G58D (by a factor of ~85) single mutants (Table 1). Thus, endogenous quality control pathways can effectively compete with the process of [*PSI*$^+$] propagation if mild inhibitors targeting different events in the Sup35 misfolding pathway are combined.

Discussion

Our studies indicate that the QNR and OPR regions make equally important but functionally distinct contributions to the efficient autocatalytic misfolding of Sup35 *in vivo* and, therefore, to the stability of the associated phenotype. Based on our analyses of the effects of Q24R and G58D expression, the QNR region is crucial for conversion to the prion form, while the OPR region determines the stability of aggregates and thereby their frangibility *in vivo*. Our observations are consistent with previous structural and genetic analyses of Sup35.[39,44,49–52] However, the PNM-induced alterations are mild (i.e. changed by a factor of ~2), suggesting that their dominant-negative effects cannot be explained simply by the failure to replicate the misfolded species. Rather, these mutations exert their effects on a

cellular level by promoting the chaperone-mediated disassembly of aggregates through different pathways: by lowering the substrate-to-enzyme ratio in the case of Q24R or by enhancing fragmentation efficiency in the case of G58D. While over-expression of Hsp104 was originally thought to induce aggregate disassembly, mounting biochemical and genetic evidence suggests that the excessive level of Hsp104 required to cure wildtype [*PSI*$^{+}$] strains is likely to act through an unknown pathway rather than through an elevated rate of fragmentation.[47,53,54] Thus, our studies are the first to demonstrate that existing aggregates can be directly and efficiently resolved by endogenous chaperones.

By uncovering the mechanism of prion curing by G58D expression, we have resolved existing conundrums in the field. First, the discrepancy in G58D effectiveness according to genetic background[40,42] can be explained by differences in levels of Hsp104, Hsp70, and Hsp40. Second, the dominant-negative effects of G58D expression had been previously reported to be conformation-specific: while G58D expression cured the Sup35 “strong” conformation ([*PSI*$^{+}$]^{Strong}), it stabilized propagation of the “weak” conformation ([*PSI*$^{+}$]^{Weak}), which is normally associated with ~3% loss.[42] [*PSI*$^{+}$]^{Weak} and [*PSI*$^{+}$]^{Strong} aggregates differ in their self-replication rates, with [*PSI*$^{+}$]^{Weak} directing more efficient conversion and less efficient fragmentation than [*PSI*$^{+}$]^{Strong}.[45] While the changes induced by G58D are clearly incompatible with [*PSI*$^{+}$]^{Strong}, these same changes specifically counteract both of the defects of [*PSI*$^{+}$]^{Weak}, providing a molecular explanation for the conformation-specific effects.[42]

Intriguingly, the correlation between effective inhibitory ratio and mechanism of interference for the PNM mutants may also hold for at least two dominant-negative PrP mutants. *In vitro*, the dominant-negative hamster PrP Q172R mutant appears to function analogously to Sup35 Q24R, converting to the prion form inefficiently and inhibiting conformational self-replication at a substoichiometric level.[27,55] In contrast, the dominant-negative hamster PrP Q219K mutant behaves with strikingly similarity to Sup35 G58D. PrP Q219K is efficiently incorporated into aggregates,[27,29,56] but this incorporation alters the physical properties of these complexes, lowering their sensitivity to proteolysis.[29] Consistent with the behavior of Sup35 G58D, PrP Q219K effectively inhibits prion propagation only when present in excess to wildtype PrP *in vitro*,[27] implying that this mutant impacts the frangibility of aggregates *in vivo*. Indeed, Q219K, like G58D, exhibits conformation-specific inhibition of prion propagation *in vivo*, acting as a dominant negative toward the less thermodynamically stable Ch/RML variant but not the more thermodynamically stable 22L variant.[28,57] These remarkable parallels between the two systems suggest that the pathways mediating prion curing by PNM mutants in yeast may provide a new framework for revealing mechanistic insight into the dominant inhibition of prion propagation in mammals.

Together, our studies suggest that the interplay between the sequence, conformation and cellular environment of a prion protein combine to determine the balance between the assembly and disassembly of aggregates and thereby the stability of the associated phenotypes. Thus, it is not simply the physical attributes of aggregates that normally preclude their resolution but rather their assembly pathway, which is too efficient to allow on-going disassembly events to effectively compete. Our observations indicate that this balance can be reversed by mild disruption of either the conversion or the fragmentation step

of the misfolding pathway *in vivo*. While attempts to cure established prion infections with externally delivered dominant-negative PrP mutants have yet to succeed in animals,[24–26] our observations of prion curing in the yeast system indicate that the combination of functionally distinct mutations or the expression of dominant-negative mutants in cells with altered chaperone levels lead to the potent inhibition of prion propagation *in vivo*. Thus, a system-based approach to prion intervention represents a potentially promising direction in which to explore future therapies.

Methods

Plasmid Construction

All plasmids generated in this study are listed in Supplementary Table 1. pRS306-P_{35}Sup35 (6686) and pRS305-P_{35}Sup35 (SB518) contain the Sup35 promoter (P_{35}) as a *Bam*HI-*Eco*RI fragment (TRS89, TRS123) and the Sup35 open reading frame (ORF) as a *Bam*HI-*Sac*I fragment (TRS17, TRS35), generated by PCR using the indicated primers (see Supplementary Table 2), subcloned into pRS306 and pRS305, respectively. All plasmids encoding Sup35 PNM mutants were created using QuickChange mutagenesis (Stratagene) according to the manufacturer's instructions using 6686 or SB659 as templates and the indicated primers (see Supplementary Table 2): G58D (SD25, SD26), Q24R (SD1, SD2), Q24K (SD33, SD34) Q24N (SD31, SD32) Q24A (SD29, SD30). pRS306-P_{tetO2}Sup35 (SB657), G58D (SB658), and Q24R (SB659) contain the ORFs as *Bam*HI-*Nae*I fragments isolated from 6686, SB467, and SB410 and subcloned into similarly digested pRS306-P_{CMV}-tTA-tetO2 (a gift from J. Laney). pRS304-Sup35 (SB641), G58D (SB642), and Q24R (SB643) contain the ORFs as *Bam*HI-*Sac*I fragments isolated from pRS306-P_{35}Sup35, SB467, and SB410, respectively, and subcloned to similarly digested pRS304. P_{35} was then subcloned into these plasmids as a *Bam*HI-*Eco*RI fragment isolated from pRS306-P_{35}Sup35 to create SB644, SB645, and SB646, respectively. pRS305-P_{35}Sup35-HA (SB629) was generated by substituting a *Pst*I-*Sal*I fragment from p316SpSup-HA3-FL (a gift from J. Weissman), which contains a fragment of Sup35 and an $(HA)_3$ epitope tag, for the corresponding region of wildtype Sup35. pRS305-P_{35}G58D-HA (SD25, SD26; SB675) and pRS305-P_{35}Q24R-HA (SD1, SD2; SB679) plasmids were generated by QuickChange mutagenesis (Stratagene) according to the manufacturer's instructions using SB629 as a template and the indicated primers. SB590 was constructed by subcloning a *Xho*I-*Sac*I fragment containing the Hsp104 promoter (P_{104}) and ORF from pHSE-Hsp104 (a gift from S. Lindquist) into similarly digested pRS426. Plasmids generated by PCR were confirmed by sequencing.

Strain Construction

All yeast strains are derivatives of 74-D694 unless otherwise noted and are listed in Supplementary Table 3. Yeast strains expressing ectopic copies of *SUP35* or PNM mutants from *URA3* (pRS306), *TRP1* (pRS304), or *LEU2* (pRS305)-based plasmids were constructed by transforming yeast strains with plasmids that were linearized with *Bst*BI, *Bsu*361, or *Afl*II, respectively, and by selecting for transformants on the appropriate minimal media. In all cases, expression was confirmed by quantitative immunoblotting for Sup35. Disruptions of *SUP35* (SD27, SD28) were generated by transformation of PCR-generated

cassettes using pFA6aKanMX4 as a template with the indicated primers (see Supplementary Table 2) and selection on complete media supplemented with G418. *HSP104* disruptions were generated by transformation of *Pvu*I-*Bam*HI fragment of pYABL5 (a gift from S. Lindquist) and selection on minimal media lacking leucine. Disruptions were verified by PCR and 2:2 segregation of the appropriate marker. *URA3* disruptions were generated by transforming M3927 (a gift from D. Stillman) that had been linearized with *Bam*HI and by selection on rich media supplemented with G418. Disruption of *URA3* was confirmed by auxotrophic phenotype. P_{35} was replaced by P_{tetO2} by transformation of PCR-generated cassettes using pCM224[58] as a template and primers (TRS218 and TRS219) and selection on complete media supplemented with G418. Replacement was confirmed by PCR, 2:2 segregation of G418 resistance, and doxycycline-induced lethality. Strains expressing GST-UGA-DsRED-NLS were constructed by transformation of *Bsu*361-digested SB531[59] and selection on minimal media lacking tryptophan.

Imaging and Fluorescence Loss In Photobleaching (FLIP)

Experiments were performed on a Zeiss LSM510-META laser scanning confocal microscope equipped with a 63× objective (NA=1.4) and an Argon/Helium Neon laser. Frames (2× zoom, 100×100 pixels, 1 Airy unit) were collected using 488-nm excitation and 500–560nm emission wavelengths for GFP-tagged proteins and 516-nm excitation and 575–615-nm emission wavelengths for DsRED-tagged proteins. Studies analyzing GST-UGA-DsRED-NLS fluorescence in zygotes were performed as previously described.[31] To quantify fluorescence intensities, nuclei from individual cells were analyzed for mean pixel intensity using ImageJ (NIH) image analysis software, and data were normalized to the wildtype mean. For FLIP, laser intensity was set to 5% for image acquisition and 100% for bleaching for 8 iterations. Cells with buds ~1/3 their size were chosen for analysis, and average fluorescence pixel intensity was monitored in the mother cell, the bud, and a nearby control cell, with bleaching of the entire bud following each image acquisition. Image analysis was performed using Zeiss LSM Image Analysis software, where specific values were normalized to background levels of fluorescence loss and presented as time post-initial bleach.

Protein Analysis

Semi-denaturing agarose gel electrophoresis, SDS-PAGE, and quantitative immunoblotting, SDS-sensitivity were performed as previously described.[59] Anti-Ssa1 rabbit serum was provided by E. Craig, and anti-Sis1 rabbit serum was provided by M. Tuite. Immunoprecipitations were performed as previously described,[60] with the following modifications. Cells were harvested in early log phase; the lysis buffer was supplemented with 5μg ml^{-1} pepstatin, Complete protease inhibitor tablet (Roche Applied Sciences), 4μl ml^{-1} Protease Inhibitor Cocktail (Sigma), and 1 mg ml^{-1} BSA, and anti-HA high affinity rat monoclonal clone 3F10 (Roche Applied Sciences) was used.

Propagon Counts

The number of propagons per cell was determined by an *in vivo* dilution, colony-based method, as previously described.[48]

Curing by Hsp104 Overexpression

Yeast strains were transformed with vector, pHSE-Hsp104 (a gift from S. Lindquist), SB590 or pLH102 (a gift from S. Lindquist) and plated on minimal medium lacking uracil. Individual colonies were transferred to YPD plates, incubated at 30°C overnight, and transferred to 5-FOA plates. Individual colonies where then isolated on ¼ YPD agarose plates. Curing was scored by the appearance of red colonies.

Supplementary Material

Refer to Web version on PubMed Central for supplementary material.

Acknowledgements

We thank J. Bender, J. Laney, B. Cox, M. Tuite, and members of the Serio, Laney and Tuite labs for helpful discussions and comments on the manuscript and S. Lindquist (Whitehead Institute), D. Stillman (The University of Utah), M. Tuite (University of Kent), E. Craig (University of Wisconsin – Madison), J. Weissman (University of California – San Francisco) and J. Laney (Brown University) for reagents. We also thank C. Klaips and B. Rock for technical assistance. This research was supported by grants from the National Institutes of Health (AG032818 to SD, GM085976 to AD, GM080907 to JAP, and GM069802 to TRS).

References

1. Tuite MF, Serio TR. The prion hypothesis: from biological anomaly to basic regulatory mechanism. Nat Rev Mol Cell Biol. 2010; 11:823–833. [PubMed: 21081963]
2. Masel J, Jansen VA, Nowak MA. Quantifying the kinetic parameters of prion replication. Biophys Chem. 1999; 77:139–152. [PubMed: 10326247]
3. Collinge J, et al. Kuru in the 21st century--an acquired human prion disease with very long incubation periods. Lancet. 2006; 367:2068–2074. [PubMed: 16798390]
4. Gambetti P, Parchi P, Petersen RB, Chen SG, Lugaresi E. Fatal familial insomnia and familial Creutzfeldt-Jakob disease: clinical, pathological and molecular features. Brain Pathol. 1995; 5:43–51. [PubMed: 7767490]
5. Webb TE, et al. Phenotypic heterogeneity and genetic modification of P102L inherited prion disease in an international series. Brain. 2008; 131:2632–2646. [PubMed: 18757886]
6. Deslys JP, et al. Genotype at codon 129 and susceptibility to Creutzfeldt-Jakob disease. Lancet. 1998; 351:1251. [PubMed: 9643750]
7. Cervenakova L, et al. Phenotype-genotype studies in kuru: implications for new variant Creutzfeldt-Jakob disease. Proc Natl Acad Sci USA. 1998; 95:13239–13241. [PubMed: 9789072]
8. Huillard d'Aignaux J, et al. Incubation period of Creutzfeldt-Jakob disease in human growth hormone recipients in France. Neurology. 1999; 53:1197–1201. [PubMed: 10522872]
9. Baker HE, et al. Aminoacid polymorphism in human prion protein and age at death in inherited prion disease. Lancet. 1991; 337:1286. [PubMed: 1674080]
10. Dickinson AG, Meikle VM, Fraser H. Identification of a gene which controls the incubation period of some strains of scrapie agent in mice. J Comp Pathol. 1968; 78:293–299. [PubMed: 4970191]
11. Carlson GA, et al. Genetics and polymorphism of the mouse prion gene complex: control of scrapie incubation time. Mol Cell Biol. 1988; 8:5528–5540. [PubMed: 3149717]
12. Shibuya S, Higuchi J, Shin RW, Tateishi J, Kitamoto T. Codon 219 Lys allele of PRNP is not found in sporadic Creutzfeldt-Jakob disease. Ann Neurol. 1998; 43:826–828. [PubMed: 9629853]
13. Goldmann W, Hunter N, Smith G, Foster J, Hope J. PrP genotype and agent effects in scrapie: change in allelic interaction with different isolates of agent in sheep, a natural host of scrapie. J Gen Virol. 1994; 75:989–995. [PubMed: 7909834]
14. Westaway D, et al. Homozygosity for prion protein alleles encoding glutamine-171 renders sheep susceptible to natural scrapie. Genes Dev. 1994; 8:959–969. [PubMed: 7926780]

15. Belt PB, et al. Identification of five allelic variants of the sheep PrP gene and their association with natural scrapie. J Gen Virol. 1995; 76:509–517. [PubMed: 7897344]
16. Clouscard C, et al. Different allelic effects of the codons 136 and 171 of the prion protein gene in sheep with natural scrapie. J Gen Virol. 1995; 76:2097–2101. [PubMed: 7636494]
17. Ikeda T, et al. Amino acid polymorphisms of PrP with reference to onset of scrapie in Suffolk and Corriedale sheep in Japan. J Gen Virol. 1995; 76:2577–2581. [PubMed: 7595361]
18. Bossers A, Schreuder BE, Muileman IH, Belt PB, Smits MA. PrP genotype contributes to determining survival times of sheep with natural scrapie. J Gen Virol. 1996; 77:2669–2673. [PubMed: 8887505]
19. Hunter N, Moore L, Hosie BD, Dingwall WS, Greig A. Association between natural scrapie and PrP genotype in a flock of Suffolk sheep in Scotland. Vet Rec. 1997; 140:59–63. [PubMed: 9023905]
20. O'Rourke KI, et al. PrP genotypes and experimental scrapie in orally inoculated Suffolk sheep in the United States. J Gen Virol. 1997; 78:975–978. [PubMed: 9129673]
21. Baylis M, et al. Scrapie epidemic in a fully PrP-genotyped sheep flock. J Gen Virol. 2002; 83:2907–2914. [PubMed: 12388827]
22. Kaneko K, et al. Evidence for protein X binding to a discontinuous epitope on the cellular prion protein during scrapie prion propagation. Proc Natl Acad Sci USA. 1997; 94:10069–10074. [PubMed: 9294164]
23. Perrier V, et al. Dominant-negative inhibition of prion replication in transgenic mice. Proc Natl Acad Sci USA. 2002; 99:13079–13084. [PubMed: 12271119]
24. Crozet C, et al. Inhibition of PrP^{Sc} formation by lentiviral gene transfer of PrP containing dominant negative mutants. J Cell Sci. 2004; 117:5591–5597. [PubMed: 15494372]
25. Furuya K, et al. Intracerebroventricular delivery of dominant negative prion protein in a mouse model of iatrogenic Creutzfeldt-Jakob disease after dura graft transplantation. Neurosci Lett. 2006; 402:222–226. [PubMed: 16759805]
26. Toupet K, et al. Effective gene therapy in a mouse model of prion diseases. PLoS ONE. 2008; 3:e2773. [PubMed: 18648643]
27. Geoghegan JC, Miller MB, Kwak AH, Harris BT, Supattapone S. Trans-dominant inhibition of prion propagation in vitro is not mediated by an accessory cofactor. PLoS Pathog. 2009; 5:e1000535. [PubMed: 19649330]
28. Atarashi R, Sim VL, Nishida N, Caughey B, Katamine S. Prion strain-dependent differences in conversion of mutant prion proteins in cell culture. J Virol. 2006; 80:7854–7862. [PubMed: 16873242]
29. Lee CI, Yang Q, Perrier V, Baskakov IV. The dominant-negative effect of the Q218K variant of the prion protein does not require protein X. Protein Sci. 2007; 16:2166–2173. [PubMed: 17766375]
30. Masel J, Jansen VA. Designing drugs to stop the formation of prion aggregates and other amyloids. Biophys Chem. 2000; 88:47–59. [PubMed: 11152275]
31. Satpute-Krishnan P, Serio TR. Prion protein remodelling confers an immediate phenotypic switch. Nature. 2005; 437:262–265. [PubMed: 16148935]
32. Satpute-Krishnan P, Langseth SX, Serio TR. Hsp104-Dependent Remodeling of Prion Complexes Mediates Protein-Only Inheritance. PLoS Biol. 2007; 5:e24. [PubMed: 17253904]
33. Ness F, Ferreira P, Cox BS, Tuite MF. Guanidine hydrochloride inhibits the generation of prion "seeds" but not prion protein aggregation in yeast. Mol Cell Biol. 2002; 22:5593–5605. [PubMed: 12101251]
34. Kawai-Noma S, Pack CG, Tsuji T, Kinjo M, Taguchi H. Single mother-daughter pair analysis to clarify the diffusion properties of yeast prion Sup35 in guanidine-HCl-treated [*PSI*] cells. Genes Cells. 2009
35. Chernoff YO, Lindquist SL, Ono B, Inge-Vechtomov SG, Liebman SW. Role of the chaperone protein Hsp104 in propagation of the yeast prion-like factor [PSI^{+}]. Science. 1995; 268:880–884. [PubMed: 7754373]

36. Tipton KA, Verges KJ, Weissman JS. In vivo monitoring of the prion replication cycle reveals a critical role for Sis1 in delivering substrates to Hsp104. Mol Cell. 2008; 32:584–591. [PubMed: 19026788]
37. Higurashi T, Hines JK, Sahi C, Aron R, Craig EA. Specificity of the J-protein Sis1 in the propagation of 3 yeast prions. Proc Natl Acad Sci USA. 2008; 105:16596–16601. [PubMed: 18955697]
38. Tessarz P, Mogk A, Bukau B. Substrate threading through the central pore of the Hsp104 chaperone as a common mechanism for protein disaggregation and prion propagation. Mol Microbiol. 2008; 68:87–97. [PubMed: 18312264]
39. DePace AH, Santoso A, Hillner P, Weissman JS. A critical role for amino-terminal glutamine/asparagine repeats in the formation and propagation of a yeast prion. Cell. 1998; 93:1241–1252. [PubMed: 9657156]
40. Doel SM, McCready SJ, Nierras CR, Cox BS. The dominant PNM2-mutation which eliminates the psi factor of Saccharomyces cerevisiae is the result of a missense mutation in the gene. Genetics. 1994; 137:659–670. [PubMed: 8088511]
41. Young C, Cox B. Extrachromosomal Elements in A Super-Suppression System of Yeast. I. A Nuclear Gene Controlling The Inheritance of the Extrachromosomal Elements. Heredity. 1971; 26:413–422.
42. Derkatch IL, Bradley ME, Zhou P, Liebman SW. The PNM2 mutation in the prion protein domain of SUP35 has distinct effects on different variants of the [*PSI*$^+$] prion in yeast. Curr Genet. 1999; 35:59–67. [PubMed: 10079323]
43. Kochneva-Pervukhova NV, et al. Mechanism of inhibition of [*PSI*$^+$] prion determinant propagation by a mutation of the N-terminus of the yeast Sup35 protein. EMBO J. 1998; 17:5805–5810. [PubMed: 9755180]
44. Osherovich LZ, Cox BS, Tuite MF, Weissman JS. Dissection and design of yeast prions. PLoS Biol. 2004; 2:E86. [PubMed: 15045026]
45. Tanaka M, Collins SR, Toyama BH, Weissman JS. The physical basis of how prion conformations determine strain phenotypes. Nature. 2006; 442:585–589. [PubMed: 16810177]
46. Derdowski A, Sindi SS, Klaips CL, DiSalvo S, Serio TR. A size threshold limits prion transmission and establishes phenotypic diversity. Science. 2010; 330:680–683. [PubMed: 21030659]
47. Kryndushkin DS, Alexandrov IM, Ter-Avanesyan MD, Kushnirov VV. Yeast [PSI$^+$] prion aggregates are formed by small Sup35 polymers fragmented by Hsp104. J Biol Chem. 2003; 278:49636–49643. [PubMed: 14507919]
48. Cox B, Ness F, Tuite M. Analysis of the generation and segregation of propagons: entities that propagate the [*PSI*$^+$] prion in yeast. Genetics. 2003; 165:23–33. [PubMed: 14504215]
49. Tessier PM, Lindquist S. Prion recognition elements govern nucleation, strain specificity and species barriers. Nature. 2007; 447:556–561. [PubMed: 17495929]
50. Krishnan R, Lindquist SL. Structural insights into a yeast prion illuminate nucleation and strain diversity. Nature. 2005; 435:765–772. [PubMed: 15944694]
51. Toyama BH, Kelly MJ, Gross JD, Weissman JS. The structural basis of yeast prion strain variants. Nature. 2007; 449:233–237. [PubMed: 17767153]
52. Santoso A, Chien P, Osherovich LZ, Weissman JS. Molecular basis of a yeast prion species barrier. Cell. 2000; 100:277–288. [PubMed: 10660050]
53. Moosavi B, Wongwigkarn J, Tuite MF. Hsp70/Hsp90 co-chaperones are required for efficient Hsp104-mediated elimination of the yeast [*PSI*$^+$] prion but not for prion propagation. Yeast. 2010; 27:167–179. [PubMed: 20014008]
54. Reidy M, Masison DC. Sti1 regulation of Hsp70 and Hsp90 is critical for curing of Saccharomyces cerevisiae [*PSI*$^+$] prions by Hsp104. Mol Cell Biol. 2010; 30:3542–3552. [PubMed: 20479121]
55. Bossers A, et al. Scrapie susceptibility-linked polymorphisms modulate the in vitro conversion of sheep prion protein to protease-resistant forms. Proc Natl Acad Sci USA. 1997; 94:4931–4936. [PubMed: 9144167]

56. Hizume M, et al. Human prion protein (PrP) 219K is converted to PrPSc but shows heterozygous inhibition in variant Creutzfeldt-Jakob disease infection. J Biol Chem. 2009; 284:3603–3609. [PubMed: 19074151]

57. Safar J, et al. Eight prion strains have PrP(Sc) molecules with different conformations. Nat Med. 1998; 4:1157–1165. [PubMed: 9771749]

58. Belli G, Gari E, Aldea M, Herrero E. Functional analysis of yeast essential genes using a promoter-substitution cassette and the tetracycline-regulatable dual expression system. Yeast. 1998; 14:1127–1138. [PubMed: 9778798]

59. Pezza JA, et al. The NatA acetyltransferase couples Sup35 prion complexes to the [*PSI*$^+$] phenotype. Mol Biol Cell. 2009; 20:1068–1080. [PubMed: 19073888]

60. Bagriantsev SN, Gracheva EO, Richmond JE, Liebman SW. Variant-specific [PSI$^+$] Infection is Transmitted by Sup35 Polymers within [*PSI*$^+$] Aggregates with Heterogeneous Protein Composition. Mol Biol Cell. 2008

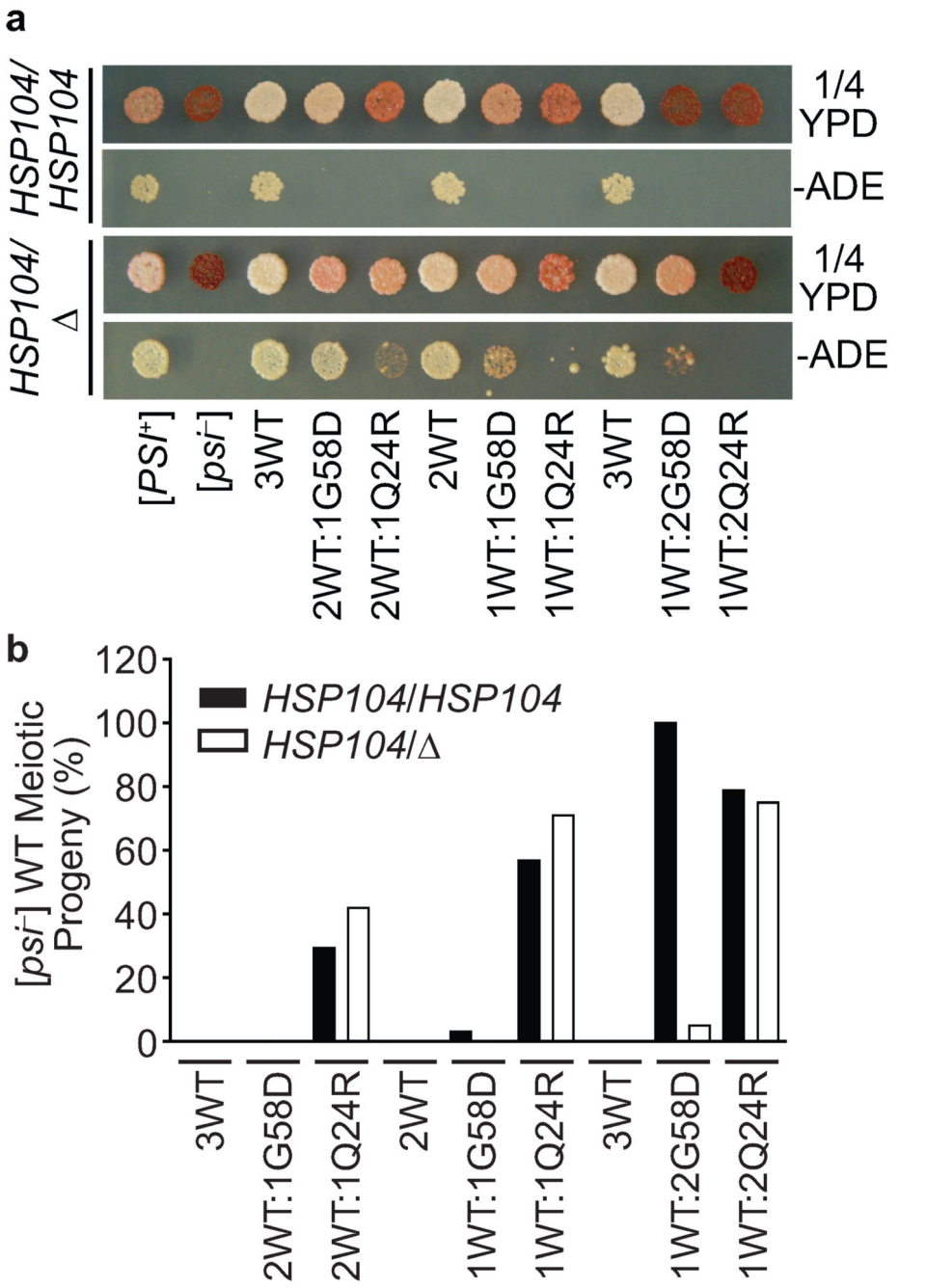

Figure 1. PNM mutants are distinguished by their effective inhibitory ratios

a. Wildtype (*HSP104/HSP104*) or heterozygous disruption (*HSP104*/Δ) diploid strains expressing wildtype (WT) and PNM mutants (Q24R, G58D) from P_{35} at the indicated ratios were spotted on rich (1/4 YPD) or adenine deficient (−ADE) media to analyze the [*PSI*$^+$] phenotype. Wildtype [*PSI*$^+$] and [*psi*$^-$] diploids (74-D694) were included as controls. **b.** To determine the frequency of prion loss, wildtype meiotic progeny (n ≥ 19 for each strain) were isolated from the diploids described in (a), and the percentage of [*psi*$^-$] colonies was determined.

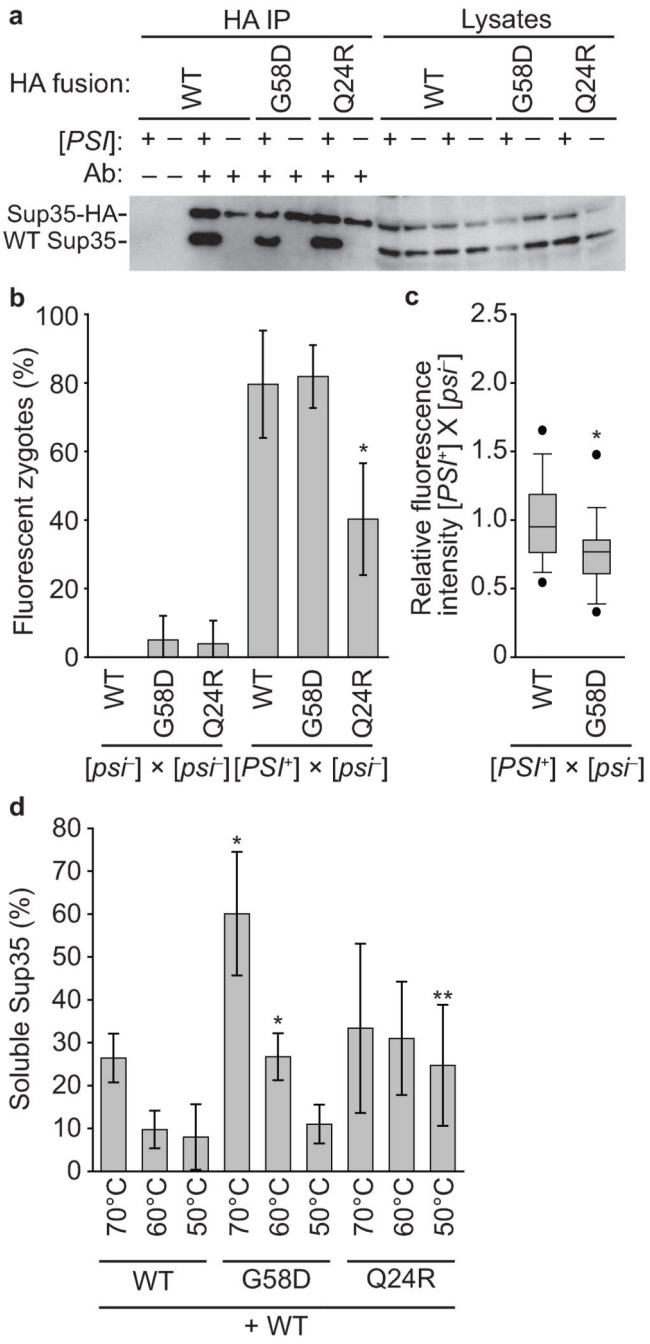

Figure 2. PNM mutants incorporate into wildtype aggregates and alter multiple events in prion propagation

a. HA-tagged Sup35 (WT or mutants) expressed from P_{35} in haploid [*PSI*$^+$] (+) or [*psi*$^-$] (−) yeast strains, which also expressed untagged Sup35, was immunoprecipitated with anti-HA serum (Ab) and analyzed by SDS-PAGE and anti-Sup35 immunoblotting. **b.** [*psi*$^-$] haploids expressing Sup35 (WT or mutants) from P_{35} and a fluorescent reporter of translation termination efficiency (GST-UGA-DsRed-NLS) were mated to wildtype [*PSI*$^+$] or [*psi*$^-$] (74-D694) cells, and the percentage of fluorescent zygotes was scored. Error bars represent

standard deviation from three independent experiments, each analyzing at least 15 zygotes per cross (*p=0.039 in comparison with WT). **c**. The fluorescence intensities of zygotes isolated from the indicated crosses as described in (b) were determined. Horizontal lines on boxes indicate 25th, 50th, and 75th percentiles; error bars indicate 10th and 90th percentiles, and dots represent outliers (n≥30; *p=0.0009). **d**. Lysates from wildtype haploid strains expressing an additional copy of Sup35 (WT or mutants) from P_{tetO2} were incubated in SDS at the indicated temperatures before SDS-PAGE and quantitative immunoblotting for Sup35 (percentage of Sup35 at the indicated temperatures relative to 100°C). Error bars represent standard deviation (n ≥ 6, *p = 0.0003, **p = 0.0001, ***p=0.008 in comparison with WT at the same temperature).

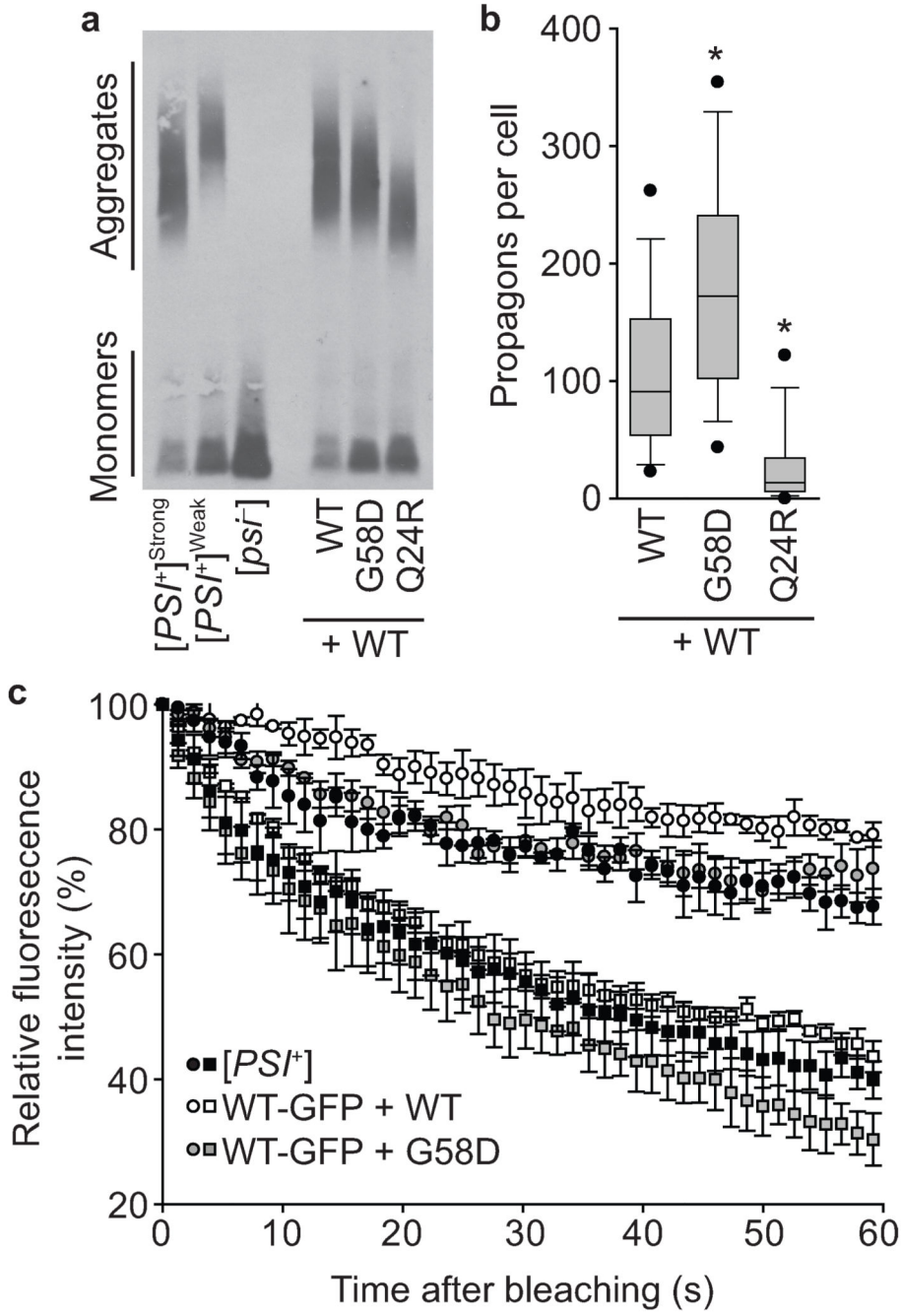

Figure 3. PNM mutants alter the accumulation of propagons but not their transmission

a. Lysates from haploid wildtype yeast strains expressing Sup35 (WT or mutants) from P_{tetO2} were analyzed by SDD-AGE and immunoblotting for Sup35. Wildtype [*PSI*$^{+}$]^{Strong}, [*PSI*$^{+}$]^{Weak}, and [*psi*$^{-}$] yeast strains are shown as controls. **b.** The number of propagons present in individual cells was determined for the indicated strains, as described in (a). Horizontal lines on boxes indicate 25th, 50th, and 75th percentiles; error bars indicate 10th and 90th percentiles, and dots represent outliers (n≥39; *p≤ 0.0001 in comparison with WT). **c**. The proportion of Sup35 transmitted to daughter cells (circles) or to mother cells (squares)

was determined by fluorescence loss in photobleaching (FLIP) of a [*PSI*$^+$] strain expressing Sup35-GFP alone ([*PSI*$^+$]) or with a second copy of Sup35 (WT-GFP + WT) or G58D (WT-GFP + G58D) from P_{tetO2}. Error bars represent standard error of the mean from three independent experiments, each analyzing at least 10 cells.

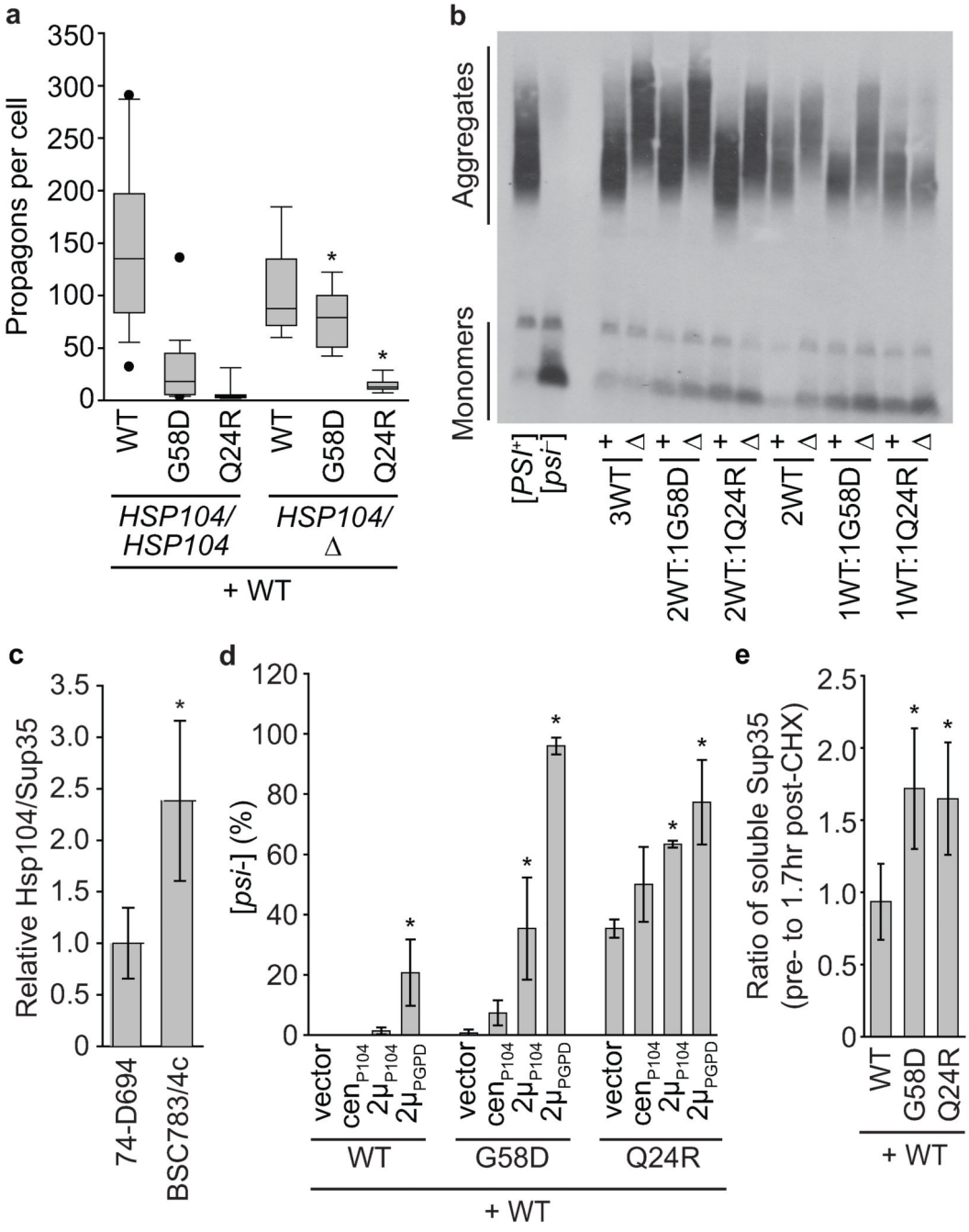

Figure 4. PNM expression promotes Hsp104-mediated disassembly of aggregates

a. The number of propagons present in individual cells was determined for diploid [*PSI*$^+$] strains expressing one endogenous copy of *SUP35* and one copy of *SUP35* (WT or mutants) from P_{tetO2} in a wildtype background (*HSP104/ HSP104*) or in a heterozygous disruption background (*HSP104/*Δ). Box plots are as described in the legend to Fig. 3b. n≥10 cells per strain; *p < 0.05, in comparison with the corresponding *HSP104/HSP104* strain. **b.** Lysates of diploid strains expressing Sup35 (WT) and PNM mutants in the indicated ratios were analyzed by SDD-AGE and immunoblotting for Sup35. Wildtype (+) and heterozygous

disruption of *HSP104* (Δ) are indicated. **c.** Lysates from BSC783/4c and 74-D694 [PSI^+] haploids were analyzed by SDS-PAGE and quantitative immunoblotting for Hsp104 and Sup35. Error bars represent standard deviation (n=5, *p=0.0031). **d**. Haploid [PSI^+] cells co-expressing endogenous *SUP35* and a second copy of *SUP35* (WT or mutants) from P_{tetO2} were transformed with pHSE-Hsp104 (cen_{P104}), SB590 ($2\mu_{P104}$), pLH102 ($2\mu_{PGPD}$) or a vector control, and the percentage of [psi^-] colonies was scored after plasmid loss. Error bars represent standard deviation from three independent experiments, each analyzing a total of 50 colonies (*p<0.05, in comparison with vector control for the same strain). **e.** Lysates from diploid [PSI^+] strains expressing two copies of *SUP35* (WT) or one wildtype and one mutant copy of *SUP35* from P_{tetO2} were incubated in SDS at 50°C or 100°C before SDS-PAGE and quantitative immunoblotting for Sup35, and the ratio of signal before and after cycloheximide treatment was determined. Error bars represent standard deviation (n≥3, *p=0.029, **p=0.011).

Table 1

Spontaneous frequencies of [*PSI*$^+$] loss during mitotic division

Strain	[*PSI*$^+$] Loss (% [*psi*$^-$])	Colonies Scored
SY1511 (WT+WT)	0	2048
SY1512 (WT+G58D)	0.35	3985
SY1513 (WT+Q24R)	5.13	3239
SY1878 (WT+Q24R/G58D)	29.76	1952